J. Fluid Mech. (2007), *vol.* 586, *pp.* 119–145. © 2007 Cambridge University Press
doi:10.1017/S0022112007006738 Printed in the United Kingdom

Conditions under which a supercritical turbidity current traverses an abrupt transition to vanishing bed slope without a hydraulic jump

SVETLANA KOSTIC AND GARY PARKER

Ven Te Chow Hydrosystems Laboratory, University of Illinois, Urbana-Champaign, IL 61801, USA
skostic@uiuc.edu; parkerg@uiuc.edu

(Received 1 February 2005 and in revised form 4 March 2007)

Turbidity currents act to sculpt the submarine environment through sediment erosion and deposition. A sufficiently swift turbidity current on a steep slope can be expected to be supercritical in the sense of the bulk Richardson number; a sufficiently tranquil turbidity current on a mild slope can be expected to be subcritical. The transition from supercritical to subcritical flow is accomplished through an internal hydraulic jump. Consider a steady turbidity current flowing from a steep canyon onto a milder fan, and then exiting the fan down another steep canyon. The flow might be expected to undergo a hydraulic jump to subcritical flow near the canyon–fan break, and then accelerate again to critical flow at the fan–canyon break downstream. The problem of locating the hydraulic jump is here termed the 'jump problem'. Experiments with fine-grained sediment have confirmed the expected behaviour outlined above. Similar experiments with coarse-grained sediment suggest that if the deposition rate is sufficiently high, this 'jump problem' may have no solution with the expected behaviour, and in particular no solution with a hydraulic jump. In such cases, the flow either transits the length of the low-slope fan as a supercritical flow and shoots off the fan–canyon break without responding to it, or dissipates as a supercritical flow before exiting the fan. The analysis presented below confirms the existence of a range associated with rapid sediment deposition where no solution to the 'jump problem' can be found. The criterion for this range is stated in terms of an order-one dimensionless parameter involving the fall velocity of the sediment. The criterion is tested and confirmed against the experiments mentioned above. A sample field application is presented.

1. Introduction

The fluid dynamics of turbidity currents, which are dense bottom underflows driven by suspended sediment, has attracted considerable interest in recent years (e.g. Hallworth, Hogg & Huppert 1998; Bonnecaze & Lister 1999; Maxworthy 1999; Gladstone & Woods 2000). Turbidity currents are close relatives of underflows driven by, for example, thermohaline effects, such as the underflow of dense, salty water across the Gibraltar Sill from the Mediterranean Sea into the Atlantic (e.g. Armi & Farmer 1988; Lane-Serff, Smeed & Postlethwaite 2000). Turbidity currents differ from such thermohaline flows in that the agent of the excess density, that is, sediment, is not a conserved quantity. Sediment is free to deposit on the bed or be entrained from it in accordance with the dictates of the flow–sediment interaction. As a result,

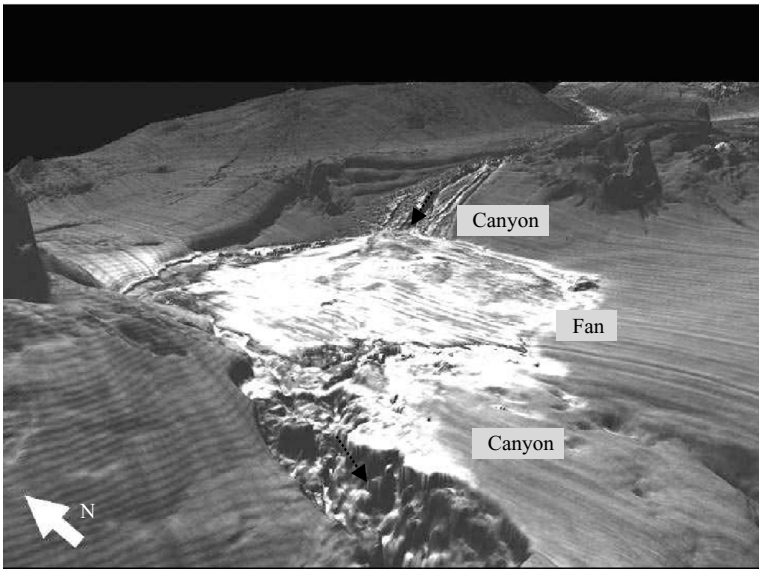

FIGURE 1. Seismic image looking upstream at a submarine canyon/fan/canyon complex on the continental slope off the Niger River, Africa. The zone between the upstream canyon and the fan is a zone of decreasing bed slope, creating conditions that could cause a turbidity current to undergo an internal hydraulic jump. The streamwise length of the fan from canyon exit to canyon entrance is about 9 km; the corresponding vertical relief is about 10 m. Image courtesy B. Prather & C. Pirmez.

turbidity currents behave differently from conservative dense bottom underflows in several key ways. This paper is devoted to one of those differences.

Turbidity currents are responsible for the creation of spectacular deep-sea morphologies. On steeper slopes, they can carve submarine canyons that are hundreds of metres deep; on shallower slopes, they can deposit submarine fans over tens or hundreds of kilometres. Figure 1 shows an example of such a morphology (Prather & Pirmez 2003). The continental slope off the delta of the Niger River, Africa shows a dip (down-slope) profile with repeated undulations in bed slope. Turbidity currents have excavated canyons into the steeper zones and deposited small submarine fans in the shallower zones. In figure 1, an upstream canyon debouches onto a fan of much lower slope; the fan ends in another canyon where slope again increases. Submarine fans may be either unchannelized or channelized. The fan in figure 1 is channelized. That is, at any given time, the flow of the turbidity current on the fan is confined to a channel, but over time the channel shifts and avulses so as to spread sediment across the entire fan. In the work reported here, the fan is assumed to be channelized. For simplicity, the channel on the fan and the channel within the canyon upstream are assumed to have the same, constant width.

A key parameter governing the dynamics of dense bottom flows is the bulk Richardson number Ri (e.g. Ellison & Turner 1959), where $Ri = RgCh/U^2$ and U denotes layer-averaged flow velocity, C denotes layer-averaged volume concentration of suspended sediment, h denotes layer thickness, g denotes the acceleration due to gravity and R denotes the submerged specific gravity of sediment, equal to 1.65 for quartz. (More formal definitions follow below.) Flows for which $Ri < 1$ are swift supercritical flows; flows for which $Ri > 1$ are tranquil subcritical flows. It is reasonable

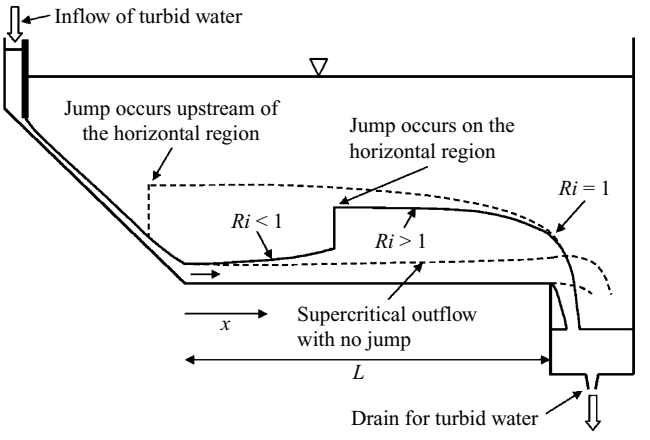

FIGURE 2. Experimental configuration of Garcia (1989).

to expect that the turbidity currents that formed the morphology of figure 1 might have been supercritical in the canyons and subcritical on the fan.

In order to make the transition from supercritical to subcritical flow, a dense bottom flow must generally undergo an internal hydraulic jump (e.g. Yih & Guha 1955). Many sedimentologists have tried to infer such jumps from the sedimentary patterns visible in outcrops (e.g. Mutti 1977; Russell & Arnott 2003). The only direct knowledge of internal hydraulic jumps due to turbidity currents, however, comes from experiments.

Perhaps the first comprehensive set of experiments on turbidity currents undergoing hydraulic jumps were those of Garcia (1989, 1993) and Garcia & Parker (1989). The configuration of the experiments is shown in figure 2. The currents were quasi-steady. They flowed from a submerged sluice gate onto a region with a bed slope S of 0.08. At a distance of 5 m from the inlet point, the bed slope dropped to zero; this region extended for another 6.6 m to a submerged free overfall, where the turbidity current debouched into a damping tank.

The geometry of figure 2 can be thought of as a one-dimensional analogue of the two-dimensional configuration of figure 1. The sloping region in figure 2 is analogous to the upstream canyon of figure 1; the horizontal region in figure 2 is analogous to the channelized fan in figure 1, and the free overfall at the downstream end of figure 2 is analogous to the canyon at the downstream end of the fan in figure 1.

Garcia (1989, 1993) used four grades of sediment in order to study the dynamics of net-depositional turbidity currents at slope breaks. In the case of the two finer grades of sediment, 4 μm material (NOVA) and 9 μm material (DAPER), supercritical flows emanating from the inlet underwent a hydraulic jump near the slope break. The subcritical flow downstream then accelerated in the vicinity of the free overfall and debouched into it. A subcritical dense underflow passing a free overfall must attain a critical Richardson number; for most purposes, this critical value can be approximated as unity. Henderson (1966) justifies this for the case of open channel flow; Turner (1973) provides the basis for the extension of the conclusion to dense underflows. The general pattern of flow observed in the NOVA and DAPER runs is schematized by the solid line of figure 2.

In the case of otherwise similar experiments with coarser sediment, i.e. 30 μm material (GLASSA), the hydraulic jump was barely, if at all, manifest. In the case of

65 μm sediment (GLASSB), a hydraulic jump was clearly absent. The absence of the hydraulic jump has been confirmed by the numerical simulations of Choi & Garcia (1995) and Kostic & Parker (2004, 2006).

One possibility is that the horizontal domain of the experiments of Garcia (1989, 1993) was too short for a hydraulic jump in the case of the coarser sediments. A second possibility, however, is that no jump is possible when the sediment is 'sufficiently coarse' in some dimensionless sense.

This speculation allows articulation of the 'jump problem'. Consider a steady supercritical turbidity current debouching onto a domain of horizontal bed ending in a free overfall. Is there any length L of the horizontal domain that allows a hydraulic jump to subcritical flow within it, such that this subcritical flow attains the critical condition in Richardson number at $x = L$?

It is shown below that for the case of a conservative dense underflow the 'jump problem' always has a solution. It is possible to specify a value of L that is too short for a hydraulic jump, in which case the supercritical flow shoots off the free overfall without responding to it, as shown in figure 2. If L is allowed to be a free variable, however, a range of values of L for which a hydraulic jump will occur on the domain can always be found.

The essential result of the analysis presented below is the conclusion that in the case of turbidity currents undergoing sufficiently rapid deposition, the 'jump problem' has no solution, regardless of the length L. In such cases, the turbidity current will either flow off the end of the domain for sufficiently short values of L, or dissipate as a supercritical flow within the domain for sufficiently long values of L. A simple dimensionless criterion discriminating between regions where the 'jump problem' has a solution and where it does not is derived.

2. Governing equations

A turbidity current is a dense bottom underflow driven by the presence of suspended sediment in the water column. The suspended sediment renders the bottom underflow denser than the ambient water above, and thus drives the current down the bottom slope. Here, the case of a turbidity current driven by a dilute suspension of sediment is considered. For simplicity, it is assumed that the flow is driven only by sediment, so that there is no difference between the temperature or salinity of the water in the underflow and the ambient water above. The ambient water is assumed to be at rest and in hydrostatic equilibrium, and is assumed to have a layer thickness that is infinite (or more precisely, at least an order of magnitude larger than the thickness of the turbidity current). This final assumption is easily justified for turbidity currents in the deep sea, where current thickness can be expected to be of the order of metres to tens of metres, whereas the depth of the ambient water above can range from a few hundreds of metres to over 4000 m (e.g. Pirmez & Imran 2003).

The equations governing a turbidity current can be expressed at a variety of levels of complexity, ranging from the box model of, for example, Gladstone & Woods (2000) to the full turbulence closure scheme of, for example, Felix (2001). Here, the layer-averaged approach of Parker, Fukushima & Pantin (1986) is employed. Let x denote a boundary-attached streamwise coordinate and y denote a coordinate orthogonal to x and thus directed upward normal from the bed. The streamwise flow velocity averaged over turbulence is denoted as u, and the volume concentration of suspended sediment averaged over turbulence is denoted as c. Since the ambient

water is in hydrostatic equilibrium, it can be assumed that $u \to 0$ and $c \to 0$ as $y \to \infty$. The flow is taken to be uniform in the transverse direction.

Layer-averaged flow velocity and concentration are denoted as U and C, respectively, where

$$U^2 h = \int_0^\infty u^2 \, \mathrm{d}y, \tag{1}$$

$$Uh = \int_0^\infty u \, \mathrm{d}y, \tag{2}$$

$$UCh = \int_0^\infty uc \, \mathrm{d}y, \tag{3}$$

and h denotes layer thickness. Parker *et al.* (1986) (see also Baines 1999) obtain the following forms for layer-integrated balance of momentum, flow mass and mass of suspended sediment:

$$\frac{\partial Uh}{\partial t} + \frac{\partial U^2 h}{\partial x} = -\tfrac{1}{2} Rg \frac{\partial Ch^2}{\partial x} + RgChS - u_*^2, \tag{4}$$

$$\frac{\partial h}{\partial t} + \frac{\partial Uh}{\partial x} = e_w U, \tag{5}$$

$$\frac{\partial Ch}{\partial t} + \frac{\partial UCh}{\partial x} = v_s(e_s - c_b). \tag{6}$$

In the above equations, S denotes streamwise bed slope and the parameter R, or submerged specific gravity of sediment, is given as

$$R = \frac{\rho_s}{\rho} - 1, \tag{7}$$

where ρ_s denotes the density of sediment and ρ denotes the density of sediment-free water. In addition, v_s denotes the fall velocity of the suspended sediment, which is characterized in terms of a single size for simplicity. The parameters u_*, e_w and e_s denote bed shear velocity, dimensionless coefficient of entrainment of ambient water from above, and dimensionless coefficient entrainment of sediment from the bed, respectively. Finally, c_b denotes a near-bed value of the local concentration averaged over turbulence c at level $y = b$, where $b/h \ll 1$. Equations (4)–(6) include several order-one shape factors. For example, the term $RgChS$ in (4) is more accurately written as $\alpha RgChS$, where

$$\alpha = \int_0^\infty f_c \, \mathrm{d}\xi, \quad f_c = \frac{c}{C}, \quad \xi = \frac{y}{h}, \tag{8}$$

All the shape factors take the value of unity for a top-hat assumption for velocity and concentration profiles, i.e.

$$\frac{u}{U} = \frac{c}{C} = \begin{cases} 1, & 0 \leqslant \xi \leqslant 1, \\ 0, & 1 < \xi. \end{cases} \tag{9}$$

Parker, Garcia & Fukushima (1987) and Garcia (1989) have evaluated the relevant shape factors for a range of experimental turbidity currents and found values not far from unity. Here, the shape factors are set to unity as a matter of simplicity.

Equations (4)–(6) are closed by means of assumptions for shear velocity u_*, coefficient of water entrainment e_w, near-bed suspended sediment concentration c_b

and coefficient of sediment entrainment e_s. Shear velocity u_* is related to layer-averaged flow velocity U by means of a dimensionless bed friction coefficient c_f, so that

$$u_*^2 = c_f U^2. \tag{10}$$

Here, c_f is approximated as a specified constant. Water entrainment is specified in terms of the empirical relation of Fukushima, Parker & Pantin (1985):

$$e_w = \frac{0.00153}{0.0204 + Ri}, \tag{11}$$

where Ri denotes a bulk Richardson number, defined as

$$Ri = \frac{RgCh}{U^2} = \frac{Rgq}{U^3}. \tag{12}$$

In (12), q denotes the volume transport rate of suspended sediment per unit width, given by the relation

$$q = UCh. \tag{13}$$

Near-bed sediment concentration c_b is related to the layer-averaged value C as

$$c_b = r_0 C, \tag{14}$$

where $r_0 \geqslant 1$ is a dimensionless coefficient, with the equality holding only for the case of the top-hat assumption. In general, r_0 is a function of the flow (Parker 1982). Here it is approximated as a constant for simplicity, an assumption that can be generalized at a future time.

Now consider the case of steady current that is free to develop in the streamwise direction. For this case, (4)–(6) reduce with the aid of (10), (13) and (14) to the following forms for gradually varied flow.

$$\frac{dU}{dx} = \frac{RiS - e_w\left(1 + \frac{1}{2}Ri\right) - c_f + \frac{1}{2}Ri\, r_0\left(1 - \dfrac{Ue_s h}{r_0 q}\right)\dfrac{v_s}{U}}{1 - Ri}\frac{U}{h} \tag{15a}$$

$$\frac{dh}{dx} = \frac{-RiS + e_w\left(2 - \frac{1}{2}Ri\right) + c_f - \frac{1}{2}Ri\, r_0\left(1 - \dfrac{Ue_s h}{r_0 q}\right)\dfrac{v_s}{U}}{1 - Ri} \tag{15b}$$

$$\frac{dq}{dx} = -r_0\frac{q}{h}\left(1 - \frac{Ue_s h}{r_0 q}\right)\frac{v_s}{U} \tag{15c}$$

The work reported here focuses on a purely depositional steady turbidity current, for which e_s vanishes. This assumption follows the tradition of a considerable body of literature on turbidity currents and related flows containing particulate material (e.g. Hallworth *et al.* 1998; Maxworthy 1999; Gladstone & Woods 2000; Kostic & Parker 2003*a*, *b*).

3. Purely depositional supercritical turbidity current flowing into a zone of vanishing bed slope

The goal of the analysis presented here is the delineation of conditions for which a steady turbidity current does not undergo a hydraulic jump near a slope break no matter how long is the length L of the horizontal region of figure 2. Now consider the configuration of the same figure 2. If a steady supercritical turbidity current is to

pass the break in slope and onto the zone of vanishing slope without undergoing a hydraulic jump to subcritical flow, it follows that the turbidity current must still be supercritical by the time it reaches the break in slope. That is, taking the origin for the streamwise coordinate to be the break in slope, it follows that

$$Ri_0 \equiv Ri|_{x=0} < 1. \tag{16}$$

Bed slope S vanishes on the domain $x \geqslant 0$. If, in addition, the turbidity current is assumed to be purely depositional ($e_s = 0$), and hatted dimensionless variables are introduced such that

$$\hat{h} = \frac{h}{h_0}, \quad \hat{U} = \frac{U}{U_0}, \quad \hat{q} = \frac{q}{q_0}, \quad \hat{x} = c_f \frac{x}{h_0}, \tag{17a–d}$$

with U_0, h_0 and q_0 corresponding to the values of U, h and q at $x = 0$, (15a–c) transform into the respective dimensionless forms

$$\frac{\mathrm{d}\hat{U}}{\mathrm{d}\hat{x}} = \frac{-1 - \dfrac{e_w}{c_f}\left(1 + \frac{1}{2}Ri_0\dfrac{\hat{q}}{\hat{U}^3}\right) + \frac{1}{2}Ri_0\dfrac{\hat{q}}{\hat{U}^4}\varphi}{1 - Ri_0\dfrac{\hat{q}}{\hat{U}^3}}\frac{\hat{U}}{\hat{h}}, \tag{18a}$$

$$\frac{\mathrm{d}\hat{h}}{\mathrm{d}\hat{x}} = \frac{1 + \dfrac{e_w}{c_f}\left(2 - \frac{1}{2}Ri_0\dfrac{\hat{q}}{\hat{U}^3}\right) - \frac{1}{2}Ri_0\dfrac{\hat{q}}{\hat{U}^4}\varphi}{1 - Ri_0\dfrac{\hat{q}}{\hat{U}^3}}, \tag{18b}$$

$$\frac{\mathrm{d}\hat{q}}{\mathrm{d}\hat{x}} = -\varphi\frac{\hat{q}}{\hat{U}\hat{h}}, \tag{18c}$$

with

$$Ri = Ri_0\frac{\hat{q}}{\hat{U}^3}, \quad Ri_0 = \frac{Rgq_0}{U_0^3} \tag{19a, b}$$

$$\varphi = r_0\frac{v_s}{c_f U_0}. \tag{20}$$

The boundary conditions on (18a–c) are

$$\hat{U}|_{\hat{x}=0} = 1, \quad \hat{h}|_{\hat{x}=0} = 1, \quad \hat{q}|_{\hat{x}=0} = 1. \tag{21a–c}$$

As shown in figure 2, the domain within which (18a–c) are to be solved ends in a free overfall located at $x = L$. If the flow does indeed undergo a jump to a subcritical flow within the domain, then the bulk Richardson number must achieve the value of unity at the overfall. That is, the following condition must be satisfied if a hydraulic jump occurs within the domain;

$$Ri|_{\hat{x}=\hat{L}} = Ri_0\left(\frac{\hat{q}}{\hat{U}^3}\right)\bigg|_{\hat{x}=\hat{L}} = 1, \tag{22}$$

where

$$\hat{L} = c_f\frac{L}{h_0}. \tag{23}$$

4. Case of a steady conservative density underflow

A conservative density underflow is one for which the agent of the density difference is conserved. The equations governing a steady conservative density underflow are

recovered from (18*a–c*) by taking the limit $v_s \to 0$ (vanishing fall velocity of the sediment), resulting in the relations

$$\frac{\mathrm{d}\hat{U}}{\mathrm{d}\hat{x}} = \frac{-1 - \dfrac{e_w}{c_f}\left(1 + \frac{1}{2}\dfrac{Ri_0}{\hat{U}^3}\right)}{1 - \dfrac{Ri_0}{\hat{U}^3}} \frac{\hat{U}}{\hat{h}}, \tag{24a}$$

$$\frac{\mathrm{d}\hat{h}}{\mathrm{d}\hat{x}} = \frac{1 + \dfrac{e_w}{c_f}\left(2 - \frac{1}{2}\dfrac{Ri_0}{\hat{U}^3}\right)}{1 - \dfrac{Ri_0}{\hat{U}^3}}, \tag{24b}$$

where since $\hat{q} = 1$ everywhere

$$Ri = \frac{Ri_0}{\hat{U}^3}. \tag{25}$$

An example of a conservative density underflow is one driven by excess density associated with thermohaline effects, in which case the following transformation is appropriate; where $\Delta\bar{\rho}$ denotes the layer-averaged excess density of the flow,

$$RC \to \frac{\Delta\bar{\rho}}{\rho}. \tag{26}$$

Although the case of a conservative density underflow has been studied extensively (e.g. Ellison & Turner 1959), it is useful to review it before progressing to the non-conservative case.

The solution of (24*a*, *b*) subject to (21*a*, *b*) on the domain of figure 2 can be implemented as follows. Assuming that e_w is specified by (11), (24*a*, *b*) can be solved subject to the boundary conditions (21*a*, *b*) for any specified value of upstream Richardson number Ri_0 and friction coefficient c_f. Here, the case $Ri_0 < 1$ (supercritical flow upstream) is considered first. It can be seen the numerator on the right-hand side of (24*a*) is always negative, whereas the denominator on the right-hand side of (24*a*) is positive. As a result, $\hat{U}$ must decrease monotonically in $\hat{x}$, in which case Ri must increase in accordance with (25). When $\hat{U}$ is reduced to the value

$$\hat{U} = (Ri_0)^{1/3}, \tag{27}$$

the Richardson number Ri attains the value unity, and the right-hand sides of both (24*a*) and (24*b*) become singular. The distance $\hat{L}_{sup\,max}$ at which this condition is reached defines the maximum possible length of a supercritical turbidity current emanating from the point $\hat{x} = 0$. Thus in general,

$$\hat{L}_{sup\,max} = \hat{L}_{sup\,max}(Ri_0, c_f). \tag{28}$$

This functional relation is shown as the lower line in figure 3 for the case $c_f = 0.005$. The numerical computations used to obtain the relation for $\hat{L}_{sup\,max}$ in figure 3, as well as all other numerical computations reported here, were done by means of a strong stability-preserving (SSP) Runge–Kutta method of third order. The algorithm satisfies the TVD property necessary to preserve monotonicity of the numerical solution and avoid unphysical oscillations that often plague the results of ordinary Runge–Kutta methods (Gottlieb, Shu & Tadmor 2001).

At any point $\hat{x}_J$ where $0 \leqslant \hat{x}_J < \hat{L}_{sup\,max}$, the current may undergo a hydraulic jump to subcritical flow. Such jumps generally entrain little ambient water (e.g. Wilkinson &

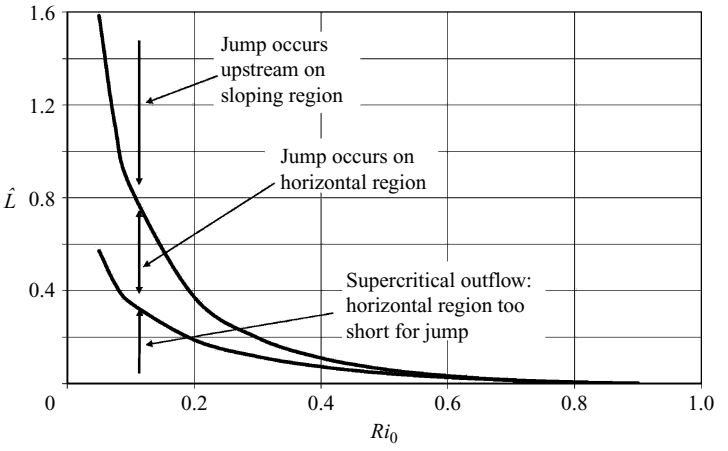

FIGURE 3. Regime diagram for the hydraulic jump of a conservative underflow, calculated for the case $c_f = 0.005$. The upper line denotes the condition $\hat{L} = \tilde{L}_{free}$, i.e. the condition for which the zone of subcritical flow is equal to the length of the domain. When $\hat{L} > \tilde{L}_{free}$, the reach downstream of the slope break of figure 2 is too long to support a hydraulic jump, and instead the flow backs up and the jump occurs upstream of the slope break in figure 2. The lower bound denotes the condition $\hat{L} = \hat{L}_{sup\,max}$, for which the supercritical flow becomes critical precisely at the overfall at the downstream end of the domain. When $\hat{L} < \hat{L}_{sup\,max}$ the supercritical flow undergoes no jump on the horizontal domain of figure 2, and remains supercritical as it shoots off the free overfall in figure 2.

Wood 1971; Stefan & Hayakawa 1972; Baddour 1987), so that the relations for conjugate Richardson number, flow velocity and flow thickness are given as

$$Ri_{cJ} = \left[\frac{\sqrt{1+8/Ri_J}-1}{2}\right]^3 Ri_J > 1, \tag{29}$$

$$\frac{\hat{U}_{cJ}}{\hat{U}_J} = \left[\frac{\sqrt{1+8/Ri_J}-1}{2}\right]^{-1} < 1, \tag{30}$$

$$\frac{\hat{h}_{cJ}}{\hat{h}_J} = \left[\frac{\sqrt{1+8/Ri_J}-1}{2}\right] > 1, \tag{31}$$

where

$$Ri_J = Ri|_{\hat{x}=\hat{x}_J}, \quad \hat{U}_J = \hat{U}|_{\hat{x}=\hat{x}_J}, \quad \hat{h}_J = \hat{h}|_{\hat{x}=\hat{x}_J} \tag{32a–c}$$

(e.g. Yih & Guha 1955). These conjugate values define the boundary conditions for the conjugate subcritical flow downstream of the jump. The governing equations for this flow may be written as

$$\frac{\mathrm{d}\tilde{U}}{\mathrm{d}\tilde{x}} = \frac{-1-\dfrac{e_w}{c_f}\left(1+\frac{1}{2}\dfrac{Ri_{cJ}}{\tilde{U}^3}\right)}{1-\dfrac{Ri_{cJ}}{\tilde{U}^3}}\frac{\tilde{U}}{\tilde{h}}, \tag{33}$$

$$\frac{\mathrm{d}\tilde{h}}{\mathrm{d}\tilde{x}} = \frac{1+\dfrac{e_w}{c_f}\left(2-\frac{1}{2}\dfrac{Ri_{cJ}}{\tilde{U}^3}\right)}{1-\dfrac{Ri_{cJ}}{\tilde{U}^3}}, \tag{34}$$

where

$$\tilde{U} = \frac{U}{U_{cJ}} = \frac{\hat{U}}{\hat{U}_{cJ}}, \quad \tilde{h} = \frac{h}{h_{cJ}} = \frac{\hat{h}}{\hat{h}_{cJ}}, \quad Ri = \frac{Ri_{cJ}}{\tilde{U}^3}, \quad \tilde{x} = \hat{x} - \hat{x}_J, \tag{35a–d}$$

and U_{cJ} and h_{cJ} denote the dimensioned conjugate flow velocity and thickness, respectively. The boundary conditions on (33) and (34) are

$$\tilde{U}|_{\tilde{x}=0} = 1, \quad \tilde{h}|_{\tilde{x}=0} = 1. \tag{36a, b}$$

Again the numerator of the right-hand side of (33) is negative, but the denominator of the same must be negative as well, at least near $\tilde{x} = 0$. As a result, $\tilde{U}$ must increase monotonically in $\tilde{x}$ until Ri attains the value unity, at which the right-hand sides of (33) and (34) become singular and the condition of a free overfall is reached. For any given values of $Ri_{cJ} > 1$ and c_f the distance $\tilde{L}_{free}$ at which the free overfall is obtained can be computed, so that

$$\tilde{L}_{free} = \tilde{L}_{free}(Ri_{cJ}, c_f). \tag{37}$$

No solution to the subcritical problem is possible over domains $\tilde{L}$ with lengths in excess of $\tilde{L}_{free}$.

Now for any value $\hat{x}_J$ satisfying the condition $0 < \hat{x}_J < \hat{L}_{sup\,max}$, a complete solution which starts with the supercritical Richardson number $Ri_0 < 1$ at $\hat{x} = 0$, undergoes a hydraulic jump at $\hat{x}_J$ and satisfies the free-overfall condition (22) at $\hat{x} = \hat{L}$, is obtained by (i) solving (24*a*) and (24*b*) subject to (21*a*) and (21*b*) from $\hat{x} = 0$ to $\hat{x} = \hat{x}_J$, (ii) computing Ri_{cJ} from (29)–(31), (iii) solving (33) and (34) subject to (36*a*) and (36*b*) from $\tilde{x} = 0$ to $\tilde{x} = \tilde{L}_{free}$ and (iv) computing $\hat{L}$ as

$$\hat{L} = \hat{x}_J + \tilde{L}(Ri_{cJ}, c_f). \tag{38}$$

For any given pair of values of $Ri_0 < 1$ and c_f and any specified value of $\hat{x}_J$, however, Ri_{cJ} can be computed as a function of $\hat{x}_J$, Ri_0 and c_f. It follows, then, that (38) reduces to the form

$$\hat{L} = \hat{L}(Ri_0, c_f, \hat{x}_J), \quad 0 \leqslant \hat{x}_J \leqslant \hat{L}_{sup\,max}. \tag{39a, b}$$

Inverting the relation of (39),

$$\hat{x}_J = \hat{x}_J(Ri_0, c_f, \hat{L}), \quad 0 \leqslant \hat{x}_J \leqslant \hat{L}_{sup\,max}. \tag{40a, b}$$

The limits in (39) and (40) have specific physical meanings. When $\hat{x}_J = 0$, the hydraulic jump occurs precisely at the slope break of figure 3, so that the conjugate Richardson number Ri_{cJ} becomes equal to the conjugate Richardson number Ri_{0J} associated with the upstream Richardson number Ri_0. In this case,

$$\hat{L} = \tilde{L}_{free}(Ri_{0J}, c_f), \tag{41a}$$

$$Ri_{0J} = \left[\frac{\sqrt{1 + 8/Ri_0} - 1}{2}\right]^3 Ri_0 > 1. \tag{41b}$$

For the case $\hat{L} > \tilde{L}_{free}(Ri_{0J}, c_f)$, it is found that $\hat{x}_J < 0$; the reach $\hat{L}$ downstream of the slope break in figure 2 is too long to support a hydraulic jump on it. Instead, the flow backs up and the jump occurs on the sloping region of figure 2 upstream of the slope break. For the case $\hat{L} < \hat{L}_{sup\,max}(Ri_0, c_f)$, on the other hand, the reach is too short for a hydraulic jump, and supercritical flow shoots off the free overfall without feeling it (figure 2).

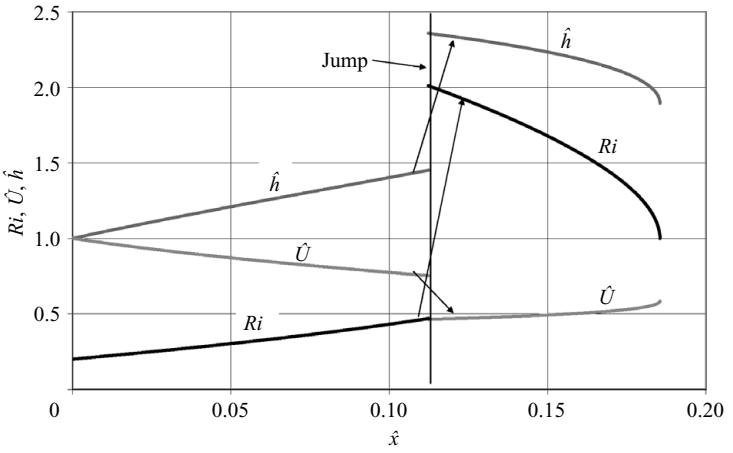

FIGURE 4. Results of a sample calculation for a conservative underflow which undergoes a hydraulic jump.

Since for the case $\hat{x}_J = 0$ the value Ri_{0J} can be computed directly from Ri_0 from (41*b*), it follows that the maximum bound on $\hat{L}$, i.e. $\hat{L}_{free}(Ri_{0J}, c_f)$ can be computed from a knowledge of Ri_0 and c_f. With this in mind, a regime diagram for the occurrence of a hydraulic jump of a conservative underflow within the domain $0 \leqslant \hat{x} \leqslant \hat{L}$ is given in figure 3, in which c_f has been set equal to 0.005 as an example.

The physical meaning of the conditions $\hat{L} > \tilde{L}_{free}$ and $\hat{L} < \hat{L}_{sup\,max}$ merit some elaboration. The condition $\hat{x}_J = 0$ locates the jump precisely at the slope break in figure 2. Between (37) and (38), then, $\hat{L} = \tilde{L}_{free}$ for this case. Forcing the condition $\hat{L} > \tilde{L}_{free}$ causes $\hat{x}_J$ to become negative in (38). In physical terms, this means that the subcritical flow calculated upstream of the free overfall is so slow and deep at the slope break of figure 2 that it creates a pressure barrier that precludes a jump there. Instead, the subcritical flow backs up onto the sloping reach, and the jump occurs upstream of the slope break. When the hydraulic jump does occur on the horizontal region of figure 2, however, it is mediated by the condition that supercritical flow is incapable of transiting the horizontal reach, i.e. $\hat{L}_{sup\,max} < \hat{L}$. That is, the supercritical flow reaches a singular state with $Ri = 1$ before the free overfall. In physical terms, then, the only way the flow can reach the free overfall is by undergoing a hydraulic jump somewhere upstream of $\hat{x} = \hat{L}_{sup\,max}$. If $\hat{L}_{sup\,max} > \hat{L}$, on the other hand, the supercritical flow can transit the horizontal domain of figure 2 without the need for a hydraulic jump. With nothing to force a jump, the supercritical flow shoots off the end of the free overfall without feeling it.

A sample calculation is given in figure 4. In the example, the values of Ri_0 and c_f are 0.2 and 0.005, respectively. For this case, the value of $\hat{L}_{sup\,max}$ is found to be 0.1872. The jump is located so as to satisfy the condition $\hat{x}_J/\hat{L}_{sup\,max} = 0.6$. The values Ri_J and Ri_{cJ} are found to be 0.469 and 2.012, respectively. The value of $\tilde{L}_{free}$ is computed as 0.0732, so that $\hat{L} = 0.6 \times 0.1872 + 0.0732 = 0.1855$. The computed profiles of Ri, $\hat{U}$ and $\hat{h}$ are given in figure 4.

For any given values of Ri_0, c_f and $\hat{L}$ it is necessary (i) to determine whether it is possible for a hydraulic jump to occur on the domain $0 \leqslant \hat{x} \leqslant \hat{L}$, and if so (ii) to iterate for the value of $\hat{x}_J$ within the bounds $0 \leqslant \hat{x}_J \leqslant \hat{L}_{sup\,max}$. The same iteration process that determines $\hat{x}_J$ also determines the solutions to (24*a*) and (24*b*) on the supercritical reach and (33) and (34) on the subcritical reach.

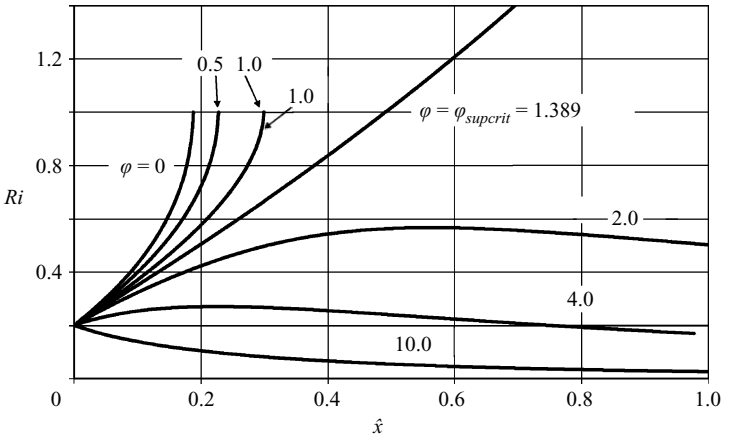

FIGURE 5. Calculations of Ri versus $\hat{x}$ for supercritical depositional turbidity currents with various values of φ, all with an upstream value $Ri_0 = 0.2$ and a value of c_f of 0.005. For $\varphi > \varphi_{supcrit}$, the turbidity current is unable to attain a value of Ri of 1 anywhere.

5. The case of a purely depositional steady turbidity current with finite fall velocity

A turbidity current differs from a conservative bottom underflow in that the agent of the density difference, i.e. sediment, can exchange with the bed through erosion and deposition. Here, the analysis of the previous section is extended to the case of a steady purely depositional turbidity current.

Supercritical flows are considered first. The equations to be solved are (18*a*)–(18*c*) subject to (21*a*)–(21*c*), and the further constraint $0 < Ri_0 < 1$. It was shown in the previous section that the case $v_s = 0$, or thus $\varphi = 0$ according to (20) has solutions such that $Ri = 1$, and the right-hand sides of (18*a*) and (18*b*) become singular at $\hat{x} = \hat{L}_{sup\,max}(Ri_0, c_f)$. It might be expected that $\hat{L}_{sup\,max}$ should change with increasing dimensionless fall velocity φ, and indeed it does. Of considerably more interest, however, is that solutions attaining $Ri = 1$ cease to exist if φ exceeds a critical value $\varphi_{supcrit}(Ri_0, c_f)$. Recalling the definition of φ from (20), the implication is that a sufficiently high fall velocity v_s (and thus deposition rate) renders a supercritical flow incapable of attaining the condition $Ri = 1$.

To see this, the case $Ri_0 = 0.2$ and $c_f = 0.005$ is considered as an example. Plots of Ri versus $\hat{x}$ are given in figure 5 for the cases $\varphi = 0$, 0.5, 1, 1.389, 2, 4 and 10. Within the range $0 < \varphi < 1.389$ it is found that solutions attaining a singularity at $Ri = 1$ do exist; the associated value $\hat{L}_{sup\,max}$ is found to be an increasing function of φ. Within the range $1.389 < \varphi$, however, a Richardson number of unity is never attained, and no singularity appears. That is, Ri first increases above Ri_0, reaches a maximum value less than unity, and thence declines monotonically toward zero.

The same general behaviour is found for any combination (Ri_0, c_f) under the constraint $Ri_0 < 1$. That is, a critical value

$$\varphi = \varphi_{supcrit}(Ri_0, c_f) \tag{42}$$

exists such that within the range $0 \leqslant \varphi < \varphi_{supcrit}$ solutions exist such that Ri attains unity at a singular point, and within the range $\varphi > \varphi_{supcrit}$ Ri never attains unity and no singularity appears. A plot of $\varphi_{supcrit}$ versus Ri_0 and c_f is given in figure 6.

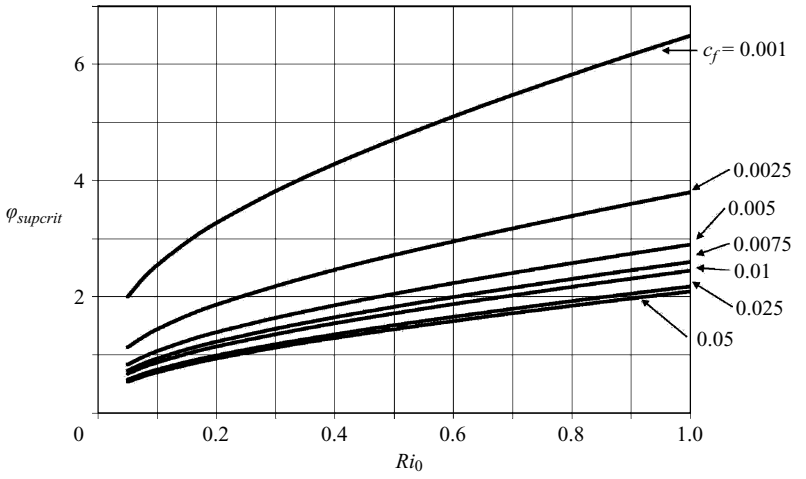

FIGURE 6. Plot of $\varphi_{supcrit}$ versus Ri_0 for various values of c_f.

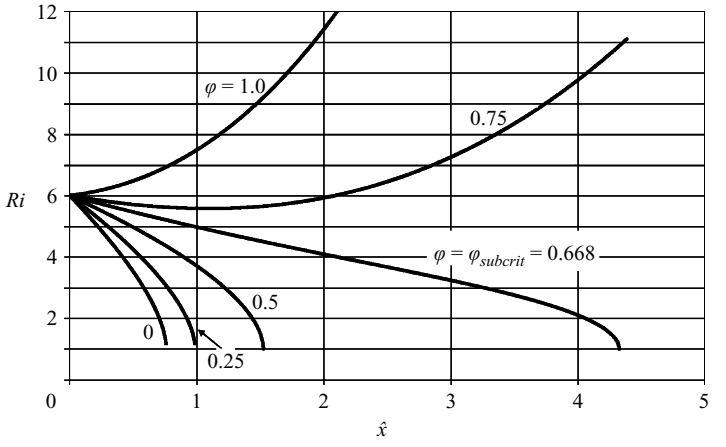

FIGURE 7. Calculations of Ri versus $\hat{x}$ for subcritical depositional turbidity currents with various values of φ, all with an upstream value of Ri of 6.00 and a value of c_f of 0.005. For $\varphi > \varphi_{subcrit}$, the turbidity current is unable to attain a value of Ri of 1 anywhere.

A point of interest with regard to figure 5 concerns the profile of Ri versus $\hat{x}$ for $\varphi = \varphi_{supcrit}$. For this value of φ and only this value, the profile passes smoothly through $Ri = 1$ without a singularity. This behaviour is found to generalize to all values of Ri_0 and c_f.

The corresponding subcritical problem is obtained by solving (18*a*)–(18*c*) subject to (21*a*)–(21*c*), and the further constraint $Ri_0 > 1$. For the case $\varphi = 0$, it was shown in the previous section that the solutions attain the value $Ri = 1$, where they become singular, at $\hat{x} = \hat{L}_{free}(Ri_0, c_f)$. (Make the transformations $\hat{x} \to \tilde{x}$, $\hat{L}_{free} = \tilde{L}_{free}$ and $Ri_0 \to Ri_{cJ}$ in comparing with the material in the previous section on subcritical flows.) Again, it is found that (i) $\hat{L}_{free}$ increases with increasing φ, and (ii) as φ increases beyond a threshold value $\varphi_{subcrit}$, the solutions fail to reach a Richardson number of unity and do not become singular anywhere. Profiles illustrating this are shown for the case $(Ri_0, c_f) = (6, 0.005)$ in figure 7; solutions become singular at $Ri = 1$ for $0 < \varphi \leqslant \varphi_{subcrit} = 0.668$, but for $\varphi > \varphi_{subcrit}$ the Richardson number attains a minimum

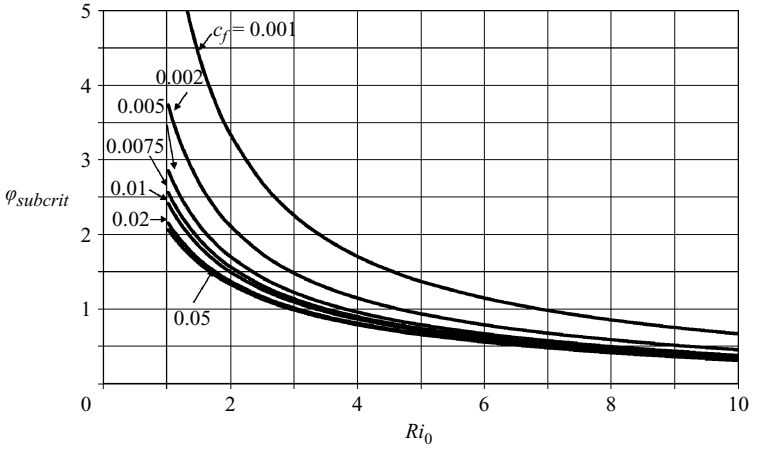

FIGURE 8. Plot of $\varphi_{subcrit}$ versus Ri_0 for various values of c_f.

value above unity, and then increases monotonically without any singularity. A plot of $\varphi_{subcrit}$ versus Ri_0 and c_f is given in figure 8.

As opposed to the case of supercritical flow, the subcritical solution remains singular at $Ri = 1$ for every value of φ for which it attains the value $Ri = 1$, including $\varphi_{subcrit}$.

Discussions of (i) the physical significance of the role of the dimensionless parameter φ in mediating the jump problem and (ii) values of φ that might be encountered in the laboratory and the field are deferred until §§ 8 and 9. It suffices to note here, however, that the parameter φ scales the effect of sediment deposition on the streamwise pressure gradient acting on the turbidity current. As explained in § 8, sediment deposition acts to hinder (i) flow deceleration in the case of supercritical flow, and (ii) flow acceleration in the case of subcritical flow.

6. Conditions for the impossibility of a hydraulic jump

The question of interest here is whether or not a steady turbidity current that is supercritical as it enters the domain $[0, L]$ of figure 2 can undergo a hydraulic jump on that domain. It is of value to review the entire formulation for the case $\varphi > 0$. In the event that a jump can occur at some point $\hat{x}_J$, the flow is supercritical in the range $0 \leqslant \hat{x} \leqslant \hat{x}_J$ and subcritical on the domain $\hat{x} > \hat{x}_J$ or $\tilde{x} > 0$. Within the supercritical range, the governing equations are (18*a*)–(18*c*) subject to (21*a*)–(21c) and the constraint $Ri_0 < 1$. Within the subcritical range, the governing equations become

$$\frac{\mathrm{d}\tilde{U}}{\mathrm{d}\tilde{x}} = \frac{-1 - \dfrac{e_w}{c_f}\left(1 + \frac{1}{2}Ri_{cJ}\dfrac{\tilde{q}}{\tilde{U}^3}\right) + \frac{1}{2}Ri_{cJ}\dfrac{\tilde{q}}{\tilde{U}^4}\tilde{\varphi}}{1 - Ri_{cJ}\dfrac{\tilde{q}}{\tilde{U}^3}}\frac{\tilde{U}}{\tilde{h}}, \tag{43a}$$

$$\frac{\mathrm{d}\tilde{h}}{\mathrm{d}\tilde{x}} = \frac{1 + \dfrac{e_w}{c_f}\left(2 - \frac{1}{2}Ri_{cJ}\dfrac{\tilde{q}}{\tilde{U}^3}\right) - \frac{1}{2}Ri_{cJ}\dfrac{\tilde{q}}{\tilde{U}^4}\tilde{\varphi}}{1 - Ri_{cJ}\dfrac{\tilde{q}}{\tilde{U}^3}}, \tag{43b}$$

$$\frac{\mathrm{d}\tilde{q}}{\mathrm{d}\tilde{x}} = -\tilde{\varphi}\frac{\tilde{q}}{\tilde{U}\tilde{h}}, \tag{43c}$$

where

$$\tilde{U} = \frac{U}{U_{cJ}} = \frac{\hat{U}}{\hat{U}_{cJ}}, \quad \tilde{h} = \frac{h}{h_{cJ}} = \frac{\hat{h}}{\hat{h}_{cJ}}, \quad \tilde{q} = \frac{q}{q_J} = \frac{\hat{q}}{\hat{q}_J}, \tag{44a–c}$$

$$Ri = \frac{Ri_{cJ}}{\tilde{U}^3}, \quad \tilde{x} = \hat{x} - \hat{x}_J, \tag{44d, e}$$

$$\tilde{\varphi} = r_0 \frac{v_s}{c_f U_{cJ}} = \frac{\varphi}{\hat{U}_{cJ}}, \tag{45}$$

$$Ri_{cJ} = \left[\frac{\sqrt{1 + 8/Ri_J} - 1}{2}\right]^3 Ri_J > 1, \tag{46a}$$

$$\frac{\hat{U}_{cJ}}{\hat{U}_J} = \left[\frac{\sqrt{1 + 8/Ri_J} - 1}{2}\right]^{-1} < 1, \tag{46b}$$

$$\frac{\hat{h}_{cJ}}{\hat{h}_J} = \left[\frac{\sqrt{1 + 8/Ri_J} - 1}{2}\right] > 1, \tag{46c}$$

$$\hat{q}_{cJ} = \hat{q}_J. \tag{46d}$$

The boundary conditions on (43) are

$$\tilde{U}|_{\tilde{x}=0} = 1, \quad \tilde{h}|_{\tilde{x}=0} = 1, \quad \tilde{q}|_{\tilde{x}=0} = 1. \tag{47a–c}$$

The problem can be posed as follows. Let the values of c_f, φ and $Ri_0 < 1$ be specified. For these values, can any value $\hat{L}$ be found such that (i) the flow undergoes a hydraulic jump within the domain $0 < \hat{x} < \hat{L}$ and (ii) the resulting subcritical flow satisfies the free overfall condition:

$$Ri|_{\hat{x}=\hat{L}} = 1 \tag{48}$$

at the downstream end of the domain?

The solution can be implemented by solving the supercritical problem of (18)–(21) starting from any value $Ri_0 < 1$ for $Ri, \hat{U}, \hat{h}$ and $\hat{q}$ as functions of $\hat{x}$, and asking whether a hydraulic jump is possible at any value $\hat{x}$. The same solution that yields $Ri, \hat{U}, \hat{h}$ and $\hat{q}$ as functions of $\hat{x}$ also yields the conjugate Richardson number Ri_c in accordance with (46*a*) and associated value $\tilde{\varphi}$ for the subcritical regime in accordance with (45) and (46*b*) (in both cases the subscript J has been omitted for simplicity). The subcritical problem is then defined by setting $\tilde{\varphi} = \tilde{\varphi}_J$ in (43) (with Ri_{cJ} equated to Ri_c).

The subcritical problem has a solution satisfying (48) only if

$$\tilde{\varphi} \leqslant \varphi_{subcrit}. \tag{49}$$

For any given value c_f, it is possible to plot $\varphi_{subcrit}$ as a function of Ri_c in accordance with figure 8. For the same value of c_f and specified values of Ri_0 and φ, the solution of (18) yields values of $\tilde{\varphi}$ and Ri_c for every admissible value of $\hat{x}$. A plot of $\tilde{\varphi}$ and $\varphi_{subcrit}$ versus Ri_c reveals whether or not a solution exists. If $\tilde{\varphi}$ plots everywhere above $\varphi_{subcrit}$, then no solution with a hydraulic jump is possible, no matter what the value of $\hat{L}$.

A sample implementation of this procedure is given in figure 9 for the case $Ri_0 = 0.3$ and $c_f = 0.005$. In addition to a plot of $\varphi_{subcrit}$ versus Ri_c, plots of $\tilde{\varphi}$ versus Ri_c are given for the cases $\varphi = 0.5, 1.0, 1.668\ (= \varphi_{supcrit})$ and 3. In the case $\varphi = 0.5$, it can be seen that $\tilde{\varphi}$ plots below $\varphi_{subcrit}$ over the entire range of values of Ri_c, indicating that a value

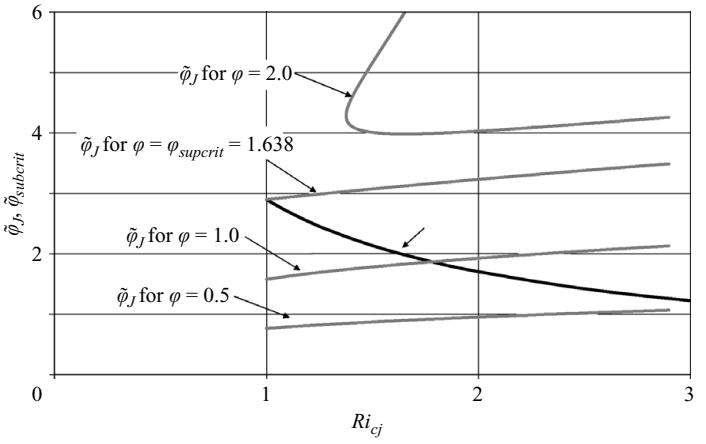

FIGURE 9. Plots of $\tilde{\varphi}_J$ versus Ri_{cJ} for various values of φ and the values $Ri_0 = 0.3$ and $c_f = 0.005$. Also plotted is $\tilde{\varphi}_J$ versus Ri_{cJ} for the case $c_f = 0.005$. No hydraulic jump to subcritical flow is possible when $\tilde{\varphi}_J > \varphi_{subcrit}$ for all Ri_{cJ}.

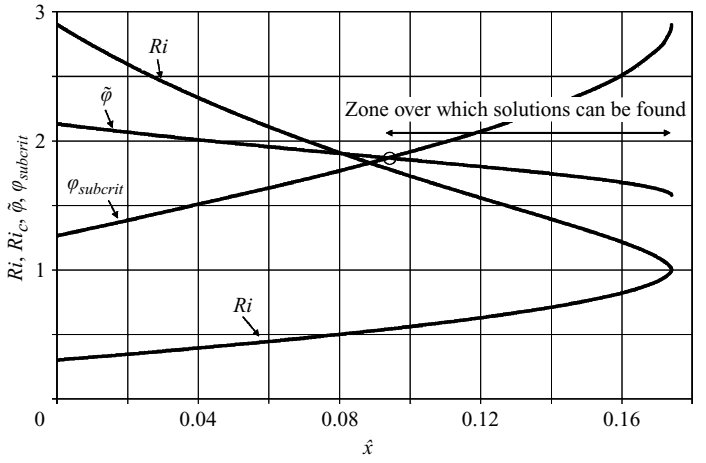

FIGURE 10. Plot of Ri, $\tilde{\varphi}$, $\varphi_{subcrit}$ and Ri_c versus $\hat{x}$ for the case $Ri_0 = 0.3$ and $c_f = 0.005$. Solutions to the jump problem can only be found only by locating the jump at a value $\hat{x} = \hat{x}_J$ for which $\tilde{\varphi} \leqslant \varphi_{subcrit}$.

$\hat{L}$ can be found such that a hydraulic jump to a subcritical flow eventually attaining the condition $Ri = 1$ is realized for all admissible values of $\hat{x}$, i.e. $0 \leqslant \hat{x} \leqslant \hat{L}_{sup\,max}$.

In the case $\varphi = 1.0$ of figure 9, however, $\tilde{\varphi}$ plots above $\varphi_{subcrit}$ for values of Ri_c above 1.78. Within this range, no hydraulic jump to a subcritical flow eventually satisfying the criterion $Ri = 1$ is possible. In figure 10, Ri, Ri_c and $\tilde{\varphi}$ of the supercritical solution are plotted versus $\hat{x}$ for the case $\varphi = 1$. In addition, the value of Ri_c is used to compute $\varphi_{subcrit}$ as a function of $\hat{x}$ for the same case of $\varphi = 1$. It can be seen that the condition (49) ensuring the existence a hydraulic jump to subcritical flow eventually attaining the condition $Ri = 1$ is satisfied only for the range $0.093 \leqslant \hat{x}_J \leqslant \hat{L}_{sup\,max}$, where in the present case $\hat{L}_{sup\,max} = 0.174$.

It is seen in figure 9 that the case $\varphi = 1.638 = \varphi_{supcrit}$ corresponds to the threshold condition for the existence of a hydraulic jump to any solution eventually reaching $Ri = 1$ for any $\hat{L}$. At this condition, the lowest value of $\tilde{\varphi}$ (at $Ri = Ri_c = 1$) of 2.90 is

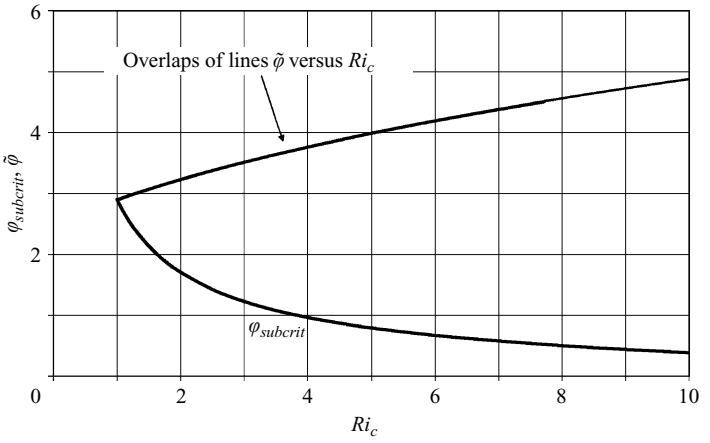

FIGURE 11. The figure shows plots of $\tilde{\varphi} = \varphi_{supcrit}(Ri_0, c_f)/\hat{U}_c[Ri_c; Ri_o, c_f, \varphi_{supcrit}(Ri_0, c_f)]$ for the case $c_f = 0.005$ and eleven values of Ri_0 (0.05, 0.1, 0.15, 0.2, 0.3, 0.4, 0.5, 0.6, 0.7, 0.8, 0.9). Also shown is the plot of $\varphi_{subcrit}$ versus Ri_c for the same value of c_f. The lines of $\tilde{\varphi}$ versus Ri_c are seen to collapse on top of each other.

precisely equal to the highest possible value of $\varphi_{subcrit}$. It is again seen from figure 9 that when $\varphi = 2 > \varphi_{supcrit}$, $\tilde{\varphi}$ exceeds $\varphi_{subcrit}$ everywhere, so that no solution with a hydraulic jump to subcritical flow eventually attaining $Ri = 1$ is possible.

The above result is an extremely simple one. The threshold value φ_{nosol} of φ above which no solution exists such that the flow (i) undergoes a hydraulic jump to subcritical flow and (ii) eventually attains the free overfall condition farther downstream can be stated as

$$\varphi_{nosol} = \varphi_{supcrit}. \tag{50}$$

The above result generalizes. In figure 11, $\tilde{\varphi}$ is plotted against Ri_c for the case $c_f = 0.005$ and the values of $Ri_0 = 0.05$, 0.075, 0.1, 0.15, 0.2, 0.3, 0.4, 0.5, 0.6, 0.7, 0.8 and 0.9, where for each value of Ri_0, φ has been set equal to the corresponding value of $\varphi_{supcrit}$. Also shown in the same plot is $\varphi_{subcrit}$ versus Ri_c. In every case, the line of $\tilde{\varphi}$ versus Ri_c plots above the curve for $\varphi_{subcrit}$ versus Ri_c, with the exception of the point $Ri_c = 1$, where $\tilde{\varphi}$ becomes equal to $\varphi_{subcrit}$. The same result was obtained for values of c_f in the range [0.001, 0.05]. Thus, figure 6, i.e. $\varphi_{supcrit}(Ri_0, c_f)$ also specifies the threshold condition above which no hydraulic jump to a subcritical flow eventually satisfying the condition $Ri = 1$ is possible.

7. Mathematical interpretation of the result

Figure 11 shows a feature that is too good to be true without reflecting some fundamental feature of the governing equations. For any given values of c_f, φ and starting value $Ri_0 < 1$ it is possible to compute $\hat{U}$, $\hat{h}$, $\hat{q}$ and Ri, and thus the conjugate values $\hat{U}_c$ and Ri_c versus $\hat{x}$ according to (18), (19*a*), (29) and (30). (Again the subscript J has been omitted here for simplicity.) The solution allows us to determine, for example, the functional relations $\hat{U}(Ri; Ri_0, c_f, \varphi)$ and $\hat{U}_c(Ri_c; Ri_0, c_f, \varphi)$. Figure 11 shows plots of the parameter $\tilde{\varphi}$ associated with the critical value $\varphi_{supcrit}$ of φ for each value of Ri_0. That is, it shows plots of

$$\tilde{\varphi} = \frac{\varphi_{supcrit}(Ri_0, c_f)}{\hat{U}_c[Ri_c; Ri_0, c_f, \varphi_{supcrit}(Ri_0, c_f)]} \tag{51}$$

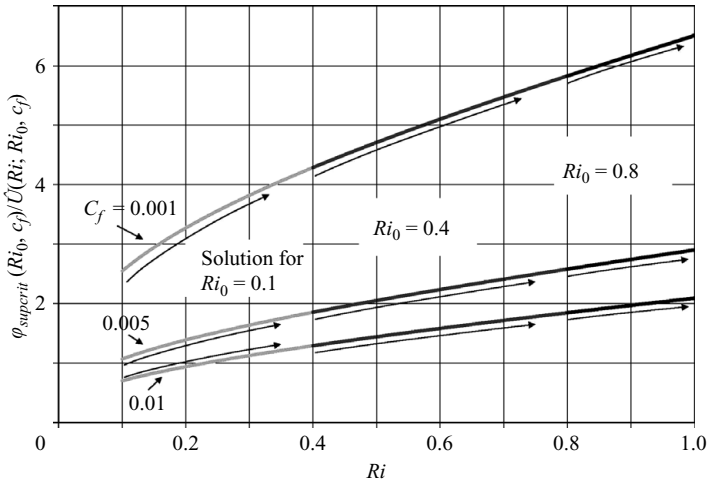

FIGURE 12. $\varphi_{supcrit}(Ri_0, c_f)/\hat{U}(Ri; Ri_0, c_f)$ against Ri for $Ri_0 = 0.1$, 0.4 and 0.8 for $c_f = 0.001$, 0.005 and 0.05. All lines are seen to collapse on top of each other for a given value of c_f.

for the case $c_f = 0.005$ and eleven values of Ri_0 ranging from 0.05 to 0.9. In all cases, the lines plot on top of each other. The values of $\tilde{\varphi}$, defining this line, plot everywhere above the maximum value of $\varphi_{subcrit}$, i.e.

$$\varphi_{subcrit,1} \equiv \varphi_{subcrit}(Ri, c_f)|_{Ri=1}, \tag{52}$$

except for the point $Ri_c = 1$, where $\tilde{\varphi} = \varphi_{subcrit,1}$.

Since Ri_c is related to Ri and $\hat{U}_c$ to $\hat{U}$ by (29) and (30), respectively, the same collapse should show up in a plot of $\varphi_{supcrit}(Ri_0, c_f)/\hat{U}(Ri; Ri_0, c_f)$. This is demonstrated in figure 12, where $\varphi_{supcrit}(Ri_0, c_f)/\hat{U}(Ri; Ri_0, c_f)$ is plotted against Ri for $Ri_0 = 0.1$, 0.4 and 0.8, and for $c_f = 0.001$, 0.005 and 0.05.

For a given c_f, the coincidence of all the lines in figures 11 and 12 for a given value of c_f is a reflection of a similarity property of the governing equations, (18). As noted in the previous section, all supercritical solutions for $\hat{U}$ and $\hat{h}$ satisfying the condition of figure 11, i.e. $\varphi = \varphi_{supcrit}(Ri_0, c_f)$ pass through $Ri = 1$ without a singularity. According to L'Hôpital's rule, the only way this can be possible in (18*a*) and (18*b*) is if the following condition is satisfied;

$$\frac{\varphi_{supcrit}(Ri_0, c_f)}{\hat{U}[Ri; Ri_0, c_f, \varphi_{supcrit}(Ri_0, c_f)]} = 2\left(1 + \frac{3}{2}\frac{e_{w1}}{c_f}\right), \tag{53}$$

where $\hat{U}_1$ is an abbreviation defined as

$$\hat{U}_1 \equiv \hat{U}[Ri; Ri_0, c_f, \varphi_{supcrit}(Ri_0, c_f)]|_{Ri=1} \tag{54}$$

and according to (11)

$$e_{w1} \equiv e_w|_{Ri=1} = 0.00150. \tag{55}$$

Of interest first is the limiting case $Ri_0 \to 1$, in which case the calculation becomes degenerate (the solution begins and ends at $\hat{x} = 0$). In this case $\hat{U}_1 = \hat{U}_{c,1} = 1$, where $\hat{U}_{c,1}$ denotes the conjugate value of $\hat{U}_1$, so that

$$\varphi_{supcrit,1} \equiv [\varphi_{supcrit}(Ri_0, c_f)]|_{Ri_0=1} = 2\left(1 + \frac{3}{2}\frac{e_{w1}}{c_f}\right). \tag{56}$$

By symmetry, it follows that

$$\varphi_{subcrit,1} = \varphi_{subcrit}(Ri, c_f)|_{Ri=1} = \varphi_{supcrit,1} = 2\left(1 + \frac{3}{2}\frac{e_{w1}}{c_f}\right). \tag{57}$$

In fact, the values of $\varphi_{supcrit}$ for the case $Ri = 1$ in figure 6 and $\varphi_{subcrit}$ for the case $Ri = 1$ in figure 8, which were obtained numerically, correspond to the predictions of (56) and (57).

Now a supercritical solution for $\hat{U}$ as a function of Ri that (i) satisfies the upstream boundary condition (18*a*) at $Ri = Ri_0$ and (ii) the condition (53) such that the solution passes through $Ri = 1$ with no singularity can be written as

$$\hat{U} = \frac{\varphi_{supcrit}(Ri_0, c_f)}{\varphi_{supcrit}(Ri, c_f)}. \tag{58}$$

In order to demonstrate that (58) is a solution, however, it also must be shown to satisfy (18). Setting $\varphi = \varphi_{supcrit}(Ri_0, c_f)$, substituting (58) into the right-hand sides of (18*a*)–(18*c*), and reducing with (19*a*), the latter equations become

$$\frac{\mathrm{d}\hat{U}}{\mathrm{d}\hat{x}} = \frac{-1 - \frac{e_w}{c_f}\left(1 + \frac{1}{2}Ri\right) + \frac{1}{2}Ri\varphi_{supcrit}(Ri, c_f)}{1 - Ri}\frac{\hat{U}}{\hat{h}}, \tag{59a}$$

$$\frac{\mathrm{d}\hat{h}}{\mathrm{d}\hat{x}} = \frac{1 + \frac{e_w}{c_f}\left(2 - \frac{1}{2}Ri\right) - \frac{1}{2}Ri\varphi_{supcrit}(Ri, c_f)}{1 - Ri}, \tag{59b}$$

$$\frac{\mathrm{d}\hat{q}}{\mathrm{d}\hat{x}} = -\varphi_{supcrit}(Ri, c_f)\frac{\hat{q}}{\hat{h}}, \tag{59c}$$

subject to the same boundary conditions as before, i.e. (21*a*–*c*). An inspection of (59*a*)–(59*c*) and (21*a*)–(21*c*) explains the collapse of the curves of figure 11 and 12 into a single line for a given value of c_f; the solution to the problem has collapsed into a single function of Ri that is independent of the upstream Richardson number Ri_0.

Further substituting (58) into the left-hand side of (59*a*) and reducing with (19*a*), it is found that

$$\begin{aligned}\frac{\mathrm{d}\hat{U}}{\mathrm{d}\hat{x}} &= -\frac{\varphi_{supcrit}(Ri_0, c_f)}{\varphi^2_{supcrit}(Ri, c_f)}\frac{\mathrm{d}\varphi_{supcrit}}{\mathrm{d}Ri}\frac{\mathrm{d}Ri}{\mathrm{d}\hat{x}} \\ &= \frac{-1 - \frac{e_w}{c_f}\left(1 + \frac{1}{2}Ri\right) + \frac{1}{2}Ri\,\varphi_{supcrit}(Ri, c_f)}{1 - Ri}\frac{1}{\hat{h}}\frac{\varphi_{supcrit}(Ri_0, c_f)}{\varphi_{supcrit}(Ri,\ c_f)}.\end{aligned} \tag{60}$$

It can be readily worked out from (18) and (19*a*) that

$$\frac{\mathrm{d}Ri}{\mathrm{d}\hat{x}} = \frac{1 + \frac{e_w}{c_f}\left(1 + \frac{1}{2}Ri\right) - \frac{1}{3}\left(1 + \frac{1}{2}Ri\right)\frac{\varphi}{\hat{U}}}{1 - Ri}. \tag{61}$$

Reducing (61) with (58) and substituting into (60), a differential equation governing $\varphi_{supcrit}$ as a function of Ri is obtained such that (58) is a solution to the problem. It

takes the form

$$\frac{\mathrm{d}\varphi_{supcrit}}{\mathrm{d}Ri} = \frac{1 + \dfrac{e_w}{c_f}\left(1 + \frac{1}{2}Ri\right) - \frac{1}{2}Ri\varphi_{supcrit}}{1 + \dfrac{e_w}{c_f}\left(1 + \frac{1}{2}Ri\right) - \frac{1}{3}\left(1 + \frac{1}{2}Ri\right)\varphi_{supcrit}}. \tag{62}$$

The above equation provides a direct way to solve for $\varphi_{supcrit}$ as a function of $Ri \leqslant 1$ for any specified value of c_f. The boundary condition on (62) is seen from (56) to be

$$\varphi_{supcrit}|_{Ri_0=1} = 2\left(1 + \frac{3}{2}\frac{e_{w1}}{c_f}\right). \tag{63}$$

As might be expected, the right-hand side of (62) is singular at $Ri = 1$, but it is easily found with the use of L'Hôpital's rule that where

$$\varphi_1' \equiv \left.\frac{\mathrm{d}\varphi_{supcrit}}{\mathrm{d}Ri}\right|_{Ri=1}, \quad \varphi_1 \equiv \varphi_{supcrit,1}, \quad r = \frac{1}{1.0204}, \tag{64}$$

the following is satisfied;

$$\varphi_1' = \frac{-\dfrac{2e_{w1}}{c_f}\left(\frac{3}{2}r - \frac{1}{2}\right) + \left\{\left[\dfrac{2e_{w1}}{c_f}\left(\frac{3}{2}r - \frac{1}{2}\right)\right]^2 + \frac{8}{3}\varphi_1\left[\dfrac{e_{w1}}{c_f}\left(\frac{3}{2}r - \frac{1}{2}\right) + \frac{1}{2}\varphi_1\right]\right\}^{1/2}}{2}. \tag{65}$$

A numerical solution of (62) subject to (63) and (65) was found to yield the curves of figure 6 (after transforming $Ri \to Ri_0$) within a fractional error of 0.002.

The curves of $\tilde{\varphi} = \varphi_{supcrit}(Ri_0, c_f)/\hat{U}_c(Ri_c; Ri_0, c_f)$ versus Ri_c in figure 11 all plot above $\varphi_{supcrit,1} = \varphi_{subcrit,1}$ for $Ri_c > 1$. From (46*b*) and (58), it is seen that

$$\tilde{\varphi} = \frac{\varphi_{supcrit}(Ri_0, c_f)}{\hat{U}_c(Ri_c; Ri_0, c_f)} = \varphi_{supcrit}(Ri, c_f)\frac{\sqrt{1 + 8/Ri} - 1}{2}. \tag{66}$$

It is easily demonstrated from (66) and the values of figure 6 that

$$\varphi_{supcrit}(Ri, c_f)\frac{\sqrt{1 + 8/Ri} - 1}{2} \geqslant \varphi_{supcrit,1}, \tag{67}$$

with the equality holding only for the case $Ri = 1$.

The criterion according to which the threshold condition for the existence of a hydraulic jump to a subcritical flow that eventually reaches a Richardson number of unity, i.e. $\varphi \leqslant \varphi_{supcrit}(Ri_0, c_f)$, is seen to be built into the structure of the governing equations.

8. Physical interpretation of the result

The existence of a critical value of $\varphi = r_0 v_s/(c_f U_0)$ above which no solution to the 'jump problem' is possible merits an explanation in terms of the governing physics. Equations (4)–(6) reduce with the aid of (10), (12)–(14), the assumption of vanishing bed slope and the neglect of erosion of bed sediment to the steady forms

$$\frac{\mathrm{d}U^2h}{\mathrm{d}x} = -\frac{1}{2}Rg\frac{\mathrm{d}}{\mathrm{d}x}\left(\frac{qh}{U}\right) - c_f U^2, \tag{68a}$$

$$\frac{\mathrm{d}Uh}{\mathrm{d}x} = e_w U, \tag{68b}$$

$$\frac{\mathrm{d}q}{\mathrm{d}x} = -r_0 v_s \frac{q}{Uh}. \tag{68c}$$

The problem of a steady conservative flow is recovered by setting $v_s = 0$. The first term on the right-hand side of (68*a*) is the term associated with the net streamwise force of the pressure gradient. Reducing it with (68*c*) yields the result

$$-\tfrac{1}{2}Rg\frac{\mathrm{d}}{\mathrm{d}x}\left(\frac{qh}{U}\right) = \tfrac{1}{2}r_0 Rg v_s \frac{q}{U^2} - \tfrac{1}{2}Rgq\frac{\mathrm{d}}{\mathrm{d}x}\left(\frac{h}{U}\right). \tag{69}$$

The first term on the right-hand side of (69) is the term that generates the possibility of no solution to the 'jump problem'. It represents a net accelerative force on the flow owing to sediment deposition. That is, as sediment deposits out of the flow in accordance with (68*c*), the streamwise pressure force per unit width $(1/2)\,\rho RgCh^2 = (1/2)\rho Rgqh/U$ declines in the streamwise direction, generating a net positive force on any control volume.

Substituting (69) back in (68*a*) yields the relation

$$\frac{\mathrm{d}U^2 h}{\mathrm{d}x} = \tfrac{1}{2}r_0 Rg v_s \frac{q}{U^2} - \tfrac{1}{2}Rgq\frac{\mathrm{d}}{\mathrm{d}x}\left(\frac{h}{U}\right) - c_f U^2, \tag{70}$$

in which the net accelerative effect on the flow owing to sediment deposition is clear. Evidently the term containing the fall velocity suppresses the ability of a supercritical flow to decelerate toward a Richardson number of unity, and likewise suppresses the ability of a subcritical flow to accelerate toward a Richardson number of unity.

To see how a net force generated by sediment deposition, which never changes sign, can suppress the ability of some flows to decelerate and others to accelerate, it is necessary to reduce (70) a bit more. A reduction of (70) with (68*b*), (68*c*) and (12) gives:

$$(1 - Ri)\frac{h}{c_f U}\frac{\mathrm{d}U}{\mathrm{d}x} = \tfrac{1}{2}Ri\frac{r_0}{c_f}\frac{v_s}{U} - \frac{e_w}{c_f}\left(1 + \tfrac{1}{2}Ri\right) - 1. \tag{71}$$

In (71) the accelerative pressure term associated with sediment deposition, i.e. the first term on the right-hand side, has not changed sign. The effect of the other pressure term, i.e. the last term on the right-hand side of (69), however, is to generate a term $(1 - Ri)$ multiplying the spatial derivative of flow velocity in (71). For a supercritical flow, $(1 - Ri)$ is positive, so that the pressure term associated with deposition adds a positive term to $\mathrm{d}U/\mathrm{d}x$ and hinders the streamwise decrease in velocity as the flow decelerates toward $Ri = 1$. For a subcritical flow, $(1 - Ri)$ is negative, so the same term hinders the streamwise increase in velocity as the flow accelerates toward $Ri = 1$. When the offending term, i.e. the first term on the right-hand side of (71), is sufficiently strong, i.e. when $\varphi > \varphi_{supcrit}$ (supercritical flow) or $\varphi > \varphi_{subcrit}$ (subcritical flow), the suppressive effect of sediment deposition is so strong that a critical Richardson number cannot be reached.

That the offending term does scale with the dimensionless parameter φ introduced in (20) can be shown by casting (71) in terms of the dimensionless variables defined in (17) and (19). The result is

$$\left(1 - Ri_0\frac{\hat{q}}{\hat{U}^3}\right)\frac{\hat{h}}{\hat{U}}\frac{\mathrm{d}\hat{U}}{\mathrm{d}\hat{x}} = \tfrac{1}{2}\varphi Ri_0\frac{\hat{q}}{\hat{U}^4} - \frac{e_w}{c_f}\left(1 + \tfrac{1}{2}Ri_0\frac{\hat{q}}{\hat{U}^3}\right) - 1. \tag{72}$$

In analogy to (71), the offending term is the first term on the right-hand side of (72).

9. Application at laboratory and field scale

The experiments of Garcia (1989) offer a means to test the criterion (50) for the occurrence of a hydraulic jump at a slope break. As noted in § 1, these experiments correspond precisely to the configuration of figure 2. Experiments were conducted with four grades of sediment, each with a different characteristic grain size D: NOVA ($D = 4\,\mu$m), DAPER ($D = 9\,\mu$m), GLASSA ($D = 30\,\mu$m) and GLASSB ($D = 65\,\mu$m), as shown in table 1. The kinematic viscosity of the water ν was computed from the water temperature θ given in the table; the fall velocity v_s for each grade was then computed from a relation of Dietrich (1982) using the values for D, R and ν in the table.

Direct measurements for the flow layer thicknesses h_0 and layer-averaged flow velocities U_0 and volume sediment concentration C_0 at the slope break of figure 2 are not reported in Garcia (1989). Kostic & Parker (2004, 2006) were, however, able to compute them upon calibrating a numerical model to the available data from Garcia (1989). Good fits to the available data were found for the value $c_f = 0.01$ for all experiments, and $r_0 = 1$ for NOVA and DAPER and $r_0 = 2$ for GLASSA and GLASSB. The computed values of h_0, U_0 and C_0 at the slope break are given in table 1, along with the assumed values of r_0. Also included in the table are the computed values of φ and $\varphi_{subcrit}$.

Garcia (1989) observed hydraulic jumps in all reported experiments using NOVA and DAPER. The formulation predicts these jumps, in that $\varphi < \varphi_{supcrit}$ in every case. Garcia did not observe hydraulic jumps in all reported experiments using GLASSA and GLASSB. The formulation again predicts the absence of jumps, in that $\varphi > \varphi_{supcrit}$ in every case.

A sample application is offered here at field scale. The numbers are loosely based on calculations for the Amazon Submarine Fan by Pirmez & Imran (2003), but have been modified to reflect relatively swift flows emanating from the Amazon Submarine Canyon. The values of (U_0, h_0, C_0, r_0, c_f, R) are taken to be (10 m s^{-1}, 50 m, 0.0124, 2.5, 0.002, 1.65); the values of Ri_0 and $\varphi_{supcrit}$ are found to be 0.10 and 1.631. As grain size is varied from 50 to 250 μm, fall velocity v_s (calculated from the relation of Dietrich 1982 at 20 °C for reference) varies from 0.22 to 3.04 cm s^{-1}, yielding values of φ ranging from 0.27 to 3.81. Based on these calculations, a hydraulic jump to Richardson-critical flow is possible only for sediment finer than about 141 μm (figure 13).

The above result applies only to a turbidity current carrying pure sand. It is likely that under some conditions a turbidity current is mostly driven by fine mud which does not readily deposit, but also carries a measurable fraction of sand which can exchange with the bed. Such a current may be able to undergo a hydraulic jump at a slope break while leaving a deposit of mostly sand.

10. Discussion

The theory presented above is formulated in the context of a layer-averaged model that employs the slender-flow approximations, i.e. the approximations that lead to the shallow-water formulation in the case of open channel flow. Such models have some limitations. One such limitation concerns the description of the internal hydraulic jump used here, i.e. that of Yih & Guha (1955). Wood & Simpson (1984), for example, have shown that the model of Yih & Guha applied to a two-layer flow of finite depth leads to the unlikely result of a (typically small but non-zero) net energy gain across the jump in the upper layer. Wood & Simpson have associated this result with the implicit assumption of hydrostatic pressure on the curved face of the jump, resulting in a slight underestimate of the force on the sloping face. They offer an

EXP.	h_0 (m)	U_0 ($m\,s^{-1}$)	$C_0 \times 10^3$	R	Ri_0	D_{50} (μm)	θ (°C)	$\nu \times 10^7$ ($m^2\,s^{-1}$)	$v_s \times 10^5$ ($m\,s^{-1}$)	r_0	φ	φ_{supcrt}	Predicted	Observed
NOVA1	0.078	0.064	0.664	1.65	0.203	4	25.5	8.93	1.15	1	0.018	1.282	Jump	Jump
NOVA2	0.065	0.071	0.985	1.65	0.208	4	25.0	9.04	1.14	1	0.016	1.295	Jump	Jump
NOVA4	0.066	0.099	2.159	1.65	0.236	4	25.0	9.04	1.14	1	0.011	1.358	Jump	Jump
DAPER1	0.078	0.061	0.671	1.65	0.225	9	26.0	8.83	7.31	1	0.119	1.333	Jump	Jump
DAPER2	0.079	0.060	0.632	1.65	0.221	9	26.0	8.83	7.31	1	0.121	1.324	Jump	Jump
DAPER4	0.063	0.085	0.132	1.65	0.187	9	26.5	8.73	7.41	1	0.088	1.244	Jump	Jump
DAPER6	0.060	0.090	1.627	1.65	0.196	9	25.5	8.93	7.21	1	0.080	1.267	Jump	Jump
DAPER7	0.060	0.101	3.344	1.65	0.318	9	23.0	9.44	6.77	1	0.067	1.526	Jump	Jump
GLASSA1	0.137	0.039	0.087	1.50	0.128	30	25.5	8.93	8.31	2	4.276	1.089	No jump	No jump
GLASSA2	0.114	0.049	0.186	1.50	0.145	30	26.0	8.83	8.40	2	3.458	1.137	No jump	No jump
GLASSA4	0.119	0.046	0.155	1.50	0.141	30	26.0	8.83	8.40	2	3.657	1.126	No jump	No jump
GLASSA5	0.110	0.051	0.218	1.50	0.149	30	26.0	8.83	8.40	2	3.289	1.148	No jump	No jump
GLASSA7	0.120	0.057	0.262	1.50	0.157	30	26.0	8.83	8.40	2	2.944	1.168	No jump	No jump
GLASSA9	0.098	0.076	0.637	1.50	0.176	30	26.5	8.73	8.50	2	2.244	1.216	No jump	No jump
GLASSB1	0.305	0.033	0.005	1.50	0.023	65	25.0	9.04	3.54	2	21.74	none	No jump	No jump
GLASSB2	0.254	0.040	0.013	1.50	0.034	65	23.5	9.34	3.44	2	17.32	0.067	No jump	No jump
GLASSB3	0.339	0.029	0.003	1.50	0.019	65	23.0	9.44	3.41	2	23.48	none	No jump	No jump

TABLE 1. Test of the criterion for a hydraulic jump versus the experimental data of Garcia (1989).

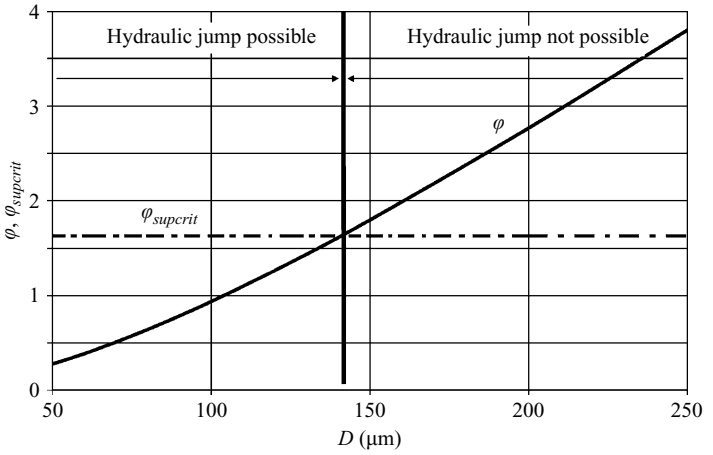

FIGURE 13. φ and $\varphi_{supcrit}$ versus grain size D for a current with the values (U_0, h_0, C_0, r_0, c_f, R) = (10 m s^{-1}, 50 m, 0.0124, 2.5, 0.002, 1.65) and a water temperature θ of 20°C. These values yield in turn the values (Ri_0, $\varphi_{supcrit}$) = (0.10, 1.631). The plot shows that a hydraulic jump to Richardson-subcritical flow is possible only for a turbidity current driven by sediment finer than about 141 μm.

alternative formulation for an internal hydraulic jump, which overcomes this defect. The case considered in the present analysis, however, is that of a turbidity current bounded above by an infinite depth of still ambient water at hydrostatic equilibrium. In this limit, the revised relation of Wood & Simpson (1984) for energy loss across the jump, i.e. (5) therein, reduces precisely to the result of Yih & Guha (1955), i.e. (7) in Wood & Simpson (1984). That is, when the upper layer is of infinite extent and at rest, there is neither energy gain nor loss in the upper layer across the jump, whereas there is always energy loss in the moving lower layer.

The present model provides an excellent predicting tool, as long as the parameters r_0 and c_f can be first calibrated to the data. Formulations that preserve the vertical structure of the flow, such as that of Imran, Kassem & Khan (2004), however, have the advantage of predicting all the structure required to infer a value of r_0. Peakall (personal communication, 2004) has pointed out that, in general, r_0 can be expected to be a function of flow conditions, as outlined in Parker (1982). A model that preserves the vertical structures of the flow allows this variation to be predicted as well.

The work presented here could thus be improved by moving from a layer-averaged model to one that includes both the vertical and transverse as well as streamwise structure of the flow. Work by Imran, Parker & Katopodes (1998), Felix (2001) and Imran *et al.* (2004), for example, suggest avenues by which these generalizations might be accomplished.

Turbidity currents can entrain bed sediment as well as deposit sediment onto the bed. That is, the sediment entrainment coefficient e_s in (6) and (15*a–c*) need not be zero. Kostic & Parker (2004, 2006) have studied the effect of including sediment entrainment in a model of the response of a turbidity current to a slope break. In correspondence to the work reported here, they have also found that sufficiently large values of the ratio v_s/U_0 cause a turbidity current to traverse a slope break of the type in figure 2 without undergoing a hydraulic jump. The similarity collapse reported in the present work can no longer be obtained, however, when sediment entrainment is included in any realistic way.

The present analysis pertains to a quasi-steady turbidity current flowing over a prescribed bed with a slope break. Over time, however, the turbidity current would gradually change the bed profile through the deposition of sediment onto (or entrainment of sediment from) the bed. This morphodynamic evolution would occur over a time scale that is much longer than that required to set up the quasi-steady flow described here. The morphodynamics of turbidity current bed interaction is considered in Kostic & Parker (2004, 2006). They have found that under the right conditions the turbidity current can leave a signature in the vicinity of the slope break in the form of a backward-facing step in the bed profile.

11. Conclusion

A one-dimensional supercritical dense bottom flow flowing from a region with a positive bed slope onto a domain of vanishing slope ending in a free overfall (figure 2) might be expected to undergo a hydraulic jump before reaching the free overfall. In the case of conservative flows driven by, for example, thermohaline effects, there is only one possible exception to this behaviour; if the length L of the horizontal reach is too short, conditions for a jump may not be reached on the domain. (If L is too long, the jump will occur on the sloping bed upstream of the transition, and the flow will no longer be supercritical at the transition.)

Turbidity currents are non-conservative dense bottom flows, in that the agent of the density difference can change owing to sediment entrainment from or deposition onto the bed. While Garcia (1989, 1993) was able to experimentally produce hydraulic jumps on the domain of figure 2 with fine-grained (4 μm and 9 μm) turbidity currents, no hydraulic jump was evident for sufficiently coarse (30 μm and 65 μm) material, even though conditions were otherwise similar. The experiments suggest that under certain conditions the physics of the problem may render a hydraulic jump impossible for any length of domain, so that the 'jump problem' described in § 1 may have no solution.

In the case of purely depositional turbidity currents, the analysis yields a critical value of the dimensionless parameter $\varphi = r_0 v_s/(c_f U_0)$, where v_s denotes sediment fall velocity, c_f denotes bed friction coefficient, U_0 denotes flow velocity at the slope break and r_0 denotes the ratio of near-bed to layer-averaged suspended sediment concentration, above which the 'jump problem' has no solution. This critical value $\varphi_{supcrit}$ is an order-one parameter that is a function of the bulk Richardson number Ri_0 at the slope break and the friction coefficient c_f.

An application of the analysis to the results of Garcia (1989, 1993) essentially confirms the results found there. In the case of the 4 μm (NOVA) and 9 μm (DAPER) sediments, the inferred values of φ fall well below the critical values above which the 'jump problem' has no solution. This corresponds with the fact that jumps were observed for these experiments. In the case of 30 μm material (GLASSA), the inferred values of φ are about twice the critical values, in agreement with the fact that no jump was observed. In the case of the 65 μm material (GLASSB), the inferred values of φ are well above the critical values, again confirming the observation that no jumps were observed. A sample calculation illustrates how the methodology of the paper can be applied at field scale.

This material is based on work supported by ExxonMobil Upstream Research Corporation and the STC Program of the National Science Foundation under Agreement Number EAR-0120914. B. E. Prather and C. Pirmez, and their parent company

Shell International Exploration and Production are sincerely thanked for introducing the authors to and allowing the reproduction of figure 1.

REFERENCES

Armi, L. & Farmer, D. 1988 The flow of Mediterranean water through the Strait of Gibraltar. *J. Phys. Oceanogr.* **21**, 1–105.

Baddour, R. E. 1987 Hydraulics of shallow and stratified mixing channel. *J. Hydraul. Engng ASCE* **113** (5), 630–645.

Baines, P. G. 1999 Downslope flows into a stratified environment – structure and detrainment. In *Mixing and Dispersion in Stably Stratified Flows* (ed. P. A. Davies), pp. 1–20. Oxford University Press.

Bonnecaze, R. T. & Lister, J. R. 1999 Particle-driven gravity currents down planar slopes. *J. Fluid Mech.* **390**, 75–91.

Choi, S. U. & Garcia, M. 1995 Modeling of one-dimensional turbidity currents with a dissipative – Galerkin finite element method. *J. Hydraul. Res.* **33**, 623–647.

Dietrich, E. W. 1982 Settling velocity of natural particles. *Water Resour. Res.* **18**, 1626–1982.

Ellison, T. H. & Turner, J. S. 1959 Turbulent entrainment in stratified flows. *J. Fluid Mech.* **6**, 423–448.

Felix, M. 2001 A two-dimensional numerical model for a turbidity current. In *Particulate Gravity Currents*, Special Publication of the International Association of Sedimentologists (ed. W. D. McCaffrey, B. C. Kneller & J. Peakall), vol. 31, pp. 71–81.

Fukushima, Y., Parker, G. & Pantin, H. M. 1985 Prediction of ignitive turbidity currents in Scripps Submarine Canyon. *Mar. Geol.* **67**, 55–81.

Garcia, M. 1989 Depositing and eroding sediment-drive flows: turbidity currents. PhD thesis, Department of Civil Engineering, University of Minnesota, Minneapolis.

Garcia, M. 1993 Hydraulic jumps in sediment-driven bottom currents. *J. Hydraul. Engng ASCE* **119** (10), 1–24.

Garcia, M. & Parker, G. 1989 Experiments on hydraulic jumps in turbidity currents near a canyonfan transition. *Science* **245**, 393–396.

Gladstone, C. & Woods, A. 2000 On the application of box models to particle-driven gravity currents. *J. Fluid Mech.* **416**, 187–195.

Gottlieb, S., Shu, C. W. & Tadmor, E. 2001 Strong stability-preserving high-order time discretization methods. *SIAM J. Numer. Anal.* **43**, 89–112.

Hallworth, M. A., Hogg, A. J. & Huppert, H. E. 1998 Effects of external flow on compositional and particle gravity currents. *J. Fluid Mech.* **359**, 109–142.

Henderson, F. M. 1966 *Open Channel Flow*. Macmillan.

Imran, J., Parker, G. & Katopodes, N. 1998 A numerical model of channel inception on submarine fans. *J. Geophys. Res. Oceans* **103** (C1), 1219–1238.

Imran, J., Kassem, A. & Khan, S. M. 2004 Three-dimensional modeling of density current. I. Flow in straight confined and unconfined channels. *J. Hydraul. Res.* **42** (6), 578–590.

Kostic, S. & Parker, G. 2003*a* Progradational sand–mud deltas in lakes and reservoirs: Part 1. Theory and numerical modeling. *J. Hydraul. Res.* **41** (2), 127–140.

Kostic, S. & Parker, G. 2003*b* Progradational sand–mud deltas in lakes and reservoirs: Part 2. Experiment and numerical simulation. *J. Hydraul. Res.* **41** (2), 141–152.

Kostic, S. & Parker, G. 2004 Can an internal hydraulic jump be inferred from the depositional record of a turbidity current? *Proceedings, RiverFlow 2004 International Conference on Fluvial Hydraulics, Napoli, Italy, June 23–25.*

Kostic, S. & Parker, G. 2006 The response of turbidity currents to a canyon–fan transition: internal hydraulic jumps and depositional signatures. *J. Hydraul. Res.* **44** (5), 631–653.

Lane-Serff, G. F., Smeed, D. A. & Postlethwaite, C. R. 2000 Multi-layer hydraulic exchange flows. *J. Fluid Mech.* **41**, 269–296.

Maxworthy, T. 1999 The dynamics of sedimenting surface gravity currents. *J. Fluid Mech.* **392**, 27–44.

Mutti, E. 1977 Distinctive thin-bedded turbidite facies and related depositional environments in the Eocene Hecho Group (South-central Pyrenees, Spain). *Sedimentology* **24**, 107–131.

PARKER, G. 1982 Conditions for the ignition of catastrophically erosive turbidity currents. *Mar. Geol.* **46**, 307–327.

PARKER, G., FUKUSHIMA, Y. & PANTIN, H. M. 1986 Self-accelerating turbidity currents. *J. Fluid Mech.* **171**, 145–181.

PARKER, G., GARCIA, M. H., FUKUSHIMA, Y. & YU, W. 1987 Experiments on turbidity currents over an erodible bed. *J. Hydraul. Res.* **25** (1), 123–147.

PIRMEZ, C. & IMRAN, J. 2003 Reconstruction of turbidity currents in a meandering submarine channel. *Mar. Petrol. Geol.* **20** (6–8), 823–849.

PRATHER, B. E. & PIRMEZ, C. 2003 Evolution of a shallow ponded basin, Niger Delta slope. *Annual Meeting Expanded Abstracts*, American Association of Petroleum Geologists **12**, 140–141.

RUSSELL, H. A. J. & ARNOTT, R. W. C. 2003 Hydraulic-jump and hyperconcentrated-flow deposits of a glacigenic subaqueous fan: Oak Ridges moraine, southern Ontario, Canada. *J. Sedimentary Res.* **73** (6), 887–905.

STEFAN, H. & HAYAKAWA, N. 1972 Mixing induced by an internal hydraulic jump. *Water Resour. Bull.* **8** (3), 531–545.

TURNER, J. S. 1973 *Buoyancy Effects in Fluids*. Cambridge University Press.

WILKINSON, D. L. & WOOD, I. R. 1971 A rapidly varied flow phenomenon in a two-layer flow. *J. Fluid Mech.* **47**, 241–256.

WOOD, I. R. & SIMPSON, J. E. 1984 Jumps in layered miscible fluids. *J. Fluid Mech.* **140**, 329–342.

YIH, C. S. & GUHA, C. R. 1955 Hydraulic jumps in a fluid system of two layers. *Tellus* **7** (3), 358–366.